Difunctional chitosan-stabilized Fe/Cu bimetallic nanoparticles for removal of hexavalent chromium wastewater

Danni Jiang [a,b,1] Danlian Huang [a,b,1] Cui Lai [a,b,1] Piao Xu [a,b,1] Guangming Zeng [a,b,*] Jia Wan [a,b] Lin Tang [a,b] Haoran Dong [a,b] Binbin Huang [a,b] Tianjue Hu [a,b]

a College of Environmental Science and Engineering, Hunan University, Changsha, 410082, PR China,

b Key Laboratory of Environmental Biology and Pollution Control, Hunan University, Ministry of Education, Changsha 410082, PR China.

Abstract

Bimetallic Fe/Cu nanoparticles were successfully stabilized by chitosan used for remediating hexavatlent chromium contaminated wastewater. However, the over-loaded chitosan on the surface of Fe/Cu particles limited the Cr(VI) reduction due to the occupation of the surface reactive sites. Weighing the colloid stability and the reduction reactivity, the optimal dosage of chitosan is 2.0wt% and the optimal Cu doping dosage is 3.0wt%. SEM and TEM images showed that the chitosan-stabilized Fe/Cu bimetallic nanoparticles (CS-Fe/Cu nanoparticles) were uniformly dispersed, which had loose and porous surface. FTIR characterization showed that the binding sites of nZVI and chitosan. XRD demonstrated that the presence of copper and chitosan did not change the existence form of zero-valent iron. Most importantly, the contribution of chitosan and Cu in the removal mechanism was studied by the reduction experiments and the XPS analysis. On the one hand, chitosan could effectively combine with Cr(VI) due to chelation, on the other hand, Cu played an important role in the precipitation and coprecipitation phenomena. These findings indicate that CS-Fe/Cu has the potential to be a promising material for wastewater treatment.

Keywords Fe/Cu nanoparticles, chitosan, hexavalent chromium, adsorption, precipitation and coprecipitation

1. Introduction

Heavy metal pollution with potential risk to human health and the environment has particularly aroused increasing public concerns due to its widespread occurrence

(Zeng et al., 2013). Among heavy metals, chromium is one of the most common toxic metal ions which mainly derive from leather tanning, electroplating, manufacturing, organic syntheses and other industries (Peng et al., 2017; Li et al., 2017a). Because of intentional and accidental release into the environment, chromium exist especially in soil and groundwater beyond the environmental standards. Chromium mainly exists in two stable valence states of Cr(III) and Cr(VI) in the environment. Cr(VI) species are soluble, mobile and bioavailability compared with Cr(III) species (Dong et al., 2017b). Therefore, it is vital to remove Cr(VI) from wastewater before discharging into the environment.

Due to their outstanding properties of easy accessibility, inexpensive and nontoxic, nanomaterials are widely used in many fields (Xu et al., 2012; Huang et al., 2016). Typically, nanoscale zero-valent iron (nZVI) particles are commonly used as an outstanding electron donor for the oxidation and transformation of a wide range of pollutants (Gong et al., 2017a; Xie et al., 2017). Compared with ZVI, the high reactivity of nZVI usually are related to the larger surface area and increased available surface reactive sites (Dong et al., 2011). However, due to the high intrinsic reactivity, the fresh nZVI tent to agglomerate rapidly and oxidize easily, which resulted in iron surface passivation. Pd (Lv et al., 2017; Li et al., 2017b; Gao et al., 2016), Ni (Dong et al., 2017a; Kumar et al., 2017; Feng and Lim, 2005), Cu (Nakseedee et al., 2017; Zeng et al., 2017; Liu et al., 2017) coating iron particles could facilitate the generation and transformation of electrons and be used for the reduction of pollutants. It is a successful strategy to enhance the reactivity of iron-based particles. In addition, in order to maintain the colloid stability, the stabilizers such as (CPC) (Liang et al., 2014; Zhou et al., 2017), starch (Kumarathilaka et al., 2016), and carboxymethyl cellulose (CMC) (Dong et al., 2017a), and guar gum (Li et al., 2016) have been commonly used. The stabilized nanoparticles existed through electrostatic repulsion and steric hindrance in the presence of stabilizer. Table.S1 summarized the modification of nZVI in recent years.

Recently, chitosan attained much attention in the green synthetic process on account of its biodegradability in the environment (Kazemi et al., 2017). Chitosan

with amine groups and hydroxyl functional groups is expected to bind strongly with Fe^0 and stabilize the nanoparticles effectively (Liu et al., 2013). Herein, we have developed a new strategy of the bimetallic Fe/Cu nanoparticles stabilized by chitosan. The system can synergistically combine two strategies: (1) chitosan for physical adsorption of Cr(VI) and (2) Cu responsible for the precipitation and coprecipitation of Cr (VI). The primary aim of this study was to (1) synthesize bimetallic Fe/Cu nanoparticles stabilized by the chitosan, and evaluate the colloid stability and chemically reactivity to determine the optimal dosage of chitosan and characterize (2) investigate the influence of different factors, such as the Cu doping dosage, the initial Cr(VI) concentration, medium pH and temperature on the Cr(VI) reduction; (3) further elucidate the role of chitosan and Cu in the Cr(VI) removal.

2. Materials and methods

2.1 Chemicals and materials

Patassium dichromate ($K_2Cr_2O_7$) and sodium borohydride ($NaHB_4$) were purchased from Sinopharm chemical Reagent Co.Ltd, Shanghai, China. Biochemical reagent grade chitosan with 95% deacetylation was purchased from Marklin Chemical Reagent Co. Ltd, Shanghai, China. All the chemical reagents used in bath experiments did not undergo any further purification. An artificial Cr(VI) contaminated solution was prepared by dissolving certain amounts of $K_2Cr_2O_7$ with ultrapure water. Ultrapure water was used throughout the whole experiment process.

2.2 Synthesis of nZVI, CS-nZVI, Fe/Cu and CS-Fe/Cu nanoparticles

Chitosan flake (0.5 g) was dissolved in 100 mL (0.5% v/v) acetic acid solution at 55°C for 5 h. Deionized water and prepared chitosan solution were pre-purged with purified N_2 for 30 min to remove O_2.

2.2.1 nZVI nanoparticles

5.6 g $FeSO_4 \cdot 7H_2O$ dissolved into 100 mL solution exclusion of dissolved oxygen. Then, 100 mL of freshly prepared $NaBH_4$ solution by dissolving 1.5132 g with dissolved oxygen ultrapure water was added to the above solution drop by drop under the condition of mechanical agitation. The obtained sample was cleaned three times

with ethanol, and then vacuum 12h at 60 ℃ to obtain the nZVI.

2.2.2 Fe/Cu nanoparticles

5.6 g $FeSO_4 \cdot 7H_2O$ dissolved into 100 mL solution exclusion of dissolved oxygen. Then, 100 mL of freshly prepared $NaBH_4$ solution by dissolving 1.5132 g with dissolved oxygen ultrapure water was added to the above solution drop by drop under the condition of mechanical agitation. Added 0.1740g $CuSO_4 \cdot 5H_2O$ into the CS-nZVI and reacted 30 min under vacuum, and then vacuum 12h at 60 ℃ to obtain the Fe/Cu nanoparticles.

2.2.3 CS-Fe nanoparticles

5.6 g $FeSO_4 \cdot 7H_2O$ dissolved into 100 mL solution exclusion of dissolved oxygen, then which was added with variable dosage chitosan solution(2wt%). Then, 100 mL of freshly prepared $NaBH_4$ solution by dissolving 1.5132 g with dissolved oxygen ultrapure water was added to the above solution drop by drop under the condition of mechanical agitation. Then vacuum 12h at 60 ℃ to obtain the CS-Fe nanoparticles.

2.2.4 CS-Fe/Cu nanoparticles

5.6 g $FeSO_4 \cdot 7H_2O$ dissolved into 100 mL solution exclusion of dissolved oxygen , then which added with variable dosage chitosan solution(1, 2, 3, 4wt%). Continuous stirring for 30 min under N_2 is needed to intensive mixing. Then, 100 mL of freshly prepared $NaBH_4$ solution by dissolving 1.5132 g with dissolved oxygen ultrapure water was added to the above solution drop by drop under the condition of mechanical agitation. Added 0.0568, 0.1136, 0.1704, 0.2272, 0.2840g $CuSO_4 \cdot 5H_2O$ into the CS-nZVI, respectively and reacted 30 min under vacuum to successfully load Cu to the CS-nZVI particles. The obtained sample was cleaned three times with ethanol, and then vacuum 12h at 60 ℃ to obtain the CS-Fe/Cu nanoparticles.

2.3 Batch experiment

Batch experiment aimed at testing the relative Cr(VI) chemical reduction reactivity of of Fe/Cu and CS-Fe/Cu was carried out. Meanwhile, tests aimed at investigating the influence of different experimental factors on the removal of Cr(VI), including

initial Cr(VI) solution concentrations, medium pH and environmental temperature. Fe^0-based nanoparticles was weighed and pour into 250 mL conical flask containing 100 mL of simulated Cr(VI) contaminated wastewater. The initial pH was adjusted in the range of 3 to 9. During the experiment, shaking bath shake at a rate of 200 rpm. At the desired reaction time, Fe/Cu and CS-Fe/Cu were magnetic separated from Cr(VI) solution, and a random 1 mL sample was extracted by 1 mL injection syringe from the supernatant for the the measurements of residual Cr(VI) concentrations. Chromium (VI) concentration was analyzed using the common diphenylcarbohydrazide method. All experiments were performed in duplicate. The removal efficiency was calculated by Eq (1):

$$\text{Cr removal efficiency (\%)} = (1-C_t/C_0)\times 100\% \quad (1)$$

Where C_t was the concentration of Cr(VI) at the specific time (mg L^{-1}), C_0 was the initial concentration of Cr(VI) (mg L^{-1}).

2.4 Characterization of stabilized nanoparticles

The synthetic material surface morphological image and elemental composition were obtained from field emission scanning electron microscope (FEI QUANTA250) with integrated energy dipersive X-ray analyser (EDX) system. The dispersibility of material was investigated using a Tecnai G2 F20 transmission electron microscope (TEM) at 200 KV. X-ray diffraction (XRD) analysis were performed on a Bruke D8 Advance (Germany) with a high-power Cu Ka X-ray source (k = 0.154 nm): at 2θ angles ranging from 10° to 80° accelerating voltage of 40 kV; emission current of 40 mA; and scanning rate of 3° 2θ per minute. Thermogravimetric measurements were performed on a STA 449 F3 Jupiter simultaneous thermal analyzer at a heating rate of 10 ℃ min^{-1} in nitrogen (Netzsth, Sellb,Germany). The X-ray photoelectron spectroscopy (XPS) characterization were recorded on a ESCALAB 250Xi (Thermo Fisher Scientific) with a monochromatic Al X-ray source at 150 w and binding energy with C1s 284.8 calibration. **3 Results and discussions**

3.1 Colloidal stability of CS-Fe/Cu nanoparticles

In order to investigate the colloidal stability of the freshly Fe/Cu suspensions in the

presence/absence of stabilizer chitosan. The kinetics study of sedimentation of Fe/Cu and CS-Fe/Cu with different loadings of chitosan as shown in Fig.1. The absorbance of 508nm was 9.22% far lower than that of 20.01% in the presence of chitosan (1 wt%) within the 60 min. This absorbance rate reduction should be related to the rapid aggregation which favored light transmittance due to intrinsic high magnetic forces (Dong et al., 2016b). It was consistent with other researchers. Dong et al (Dong et al., 2016a) reported that the absorbance of 508 nm weaken by almost 60% within 10 min due to pristine nZVI particles aggregation. In comparison, the absorbance at 508 nm changed from 20.01% to 30.22% along with increased chitosan concentration from 1.0 to 4.0wt%, in other words, the colloidal stability of CS-Fe/Cu were under the control of chitosan loadings. The above results suggested that chitosan played a vital role in dispersing the Fe-Cu nanoparticles. It was reported that stretching frequencies of the N and O atoms from the N-H and O-H functional groups vibration of chitosan are expected to shift significantly due to the Fe^0 particles attachment (Xie et al., 2016). To summarize, the concentration of chitosan is expected to affect the crystal nucleation and aggregation of the Fe/Cu particles, and the more chitosan loadings resulted in the more evenly dispersion of CS-Fe/Cu nanoparticles.

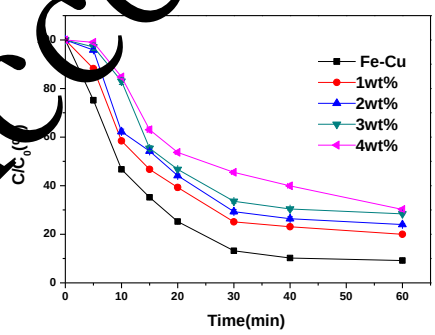

Fig.1. Kinetics study of sedimentation of Fe/Cu, CS-Fe/Cu with different dosages of chitosan.

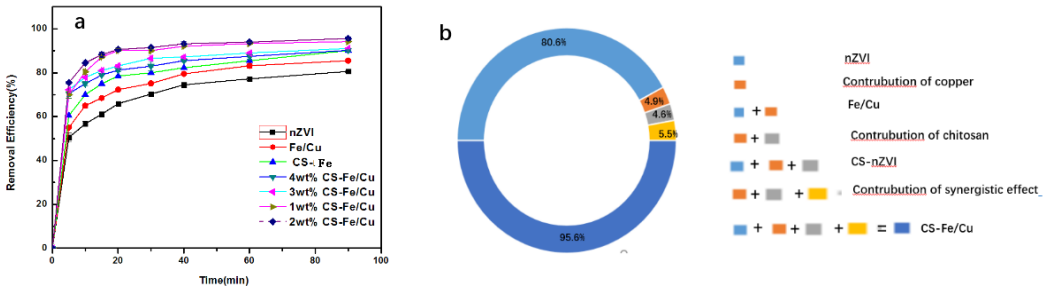

Fig.2. (a) Cr(VI) removal efficiency by nZVI; Fe/Cu; ; CS-Fe/Cu under different dosages of chitosan; (b) the contribution of Cu, chitosan, Cu and chitosan in the Cr(VI) removal.

3.2 Reduction activity of CS-Fe/Cu nanoparticles

Cr(VI) reduction batch experiments aimed at the comparation of reduction efficiency between different iron-based nanoparticles, the initial concentrations of nZVI and Cr(VI) were 200 mg/L and 20 mg/L, respectively.

The removal efficiency of Cr(VI) and contribution of various materials were shown in Fig. 2, Cr(VI) removal efficiency come up to 80.6%, 85.5% 90.1% and 95.6% by nZVI, Fe/Cu, CS-Fe and CS-Fe/Cu, respectively. The poor removal efficiency utilizing nZVI was caused by the formation of passive layer on the surface of particles (Arancibid-Miranda et al., 2017). On one hand, the removal efficiency of Cr(VI) significantly improved from 80.6% to 95.6% with the increasing dosage of chitosan from 0 to 2 wt%. This was consistent with other researchers. Dong et al reported that polyacrylic acid (PAA) molecules on the surface of nZVI nanoparticles changed the surface charge, and thereby electrostatic repulsion prevented the nanopartilces from aggregation in the range from 1wt% to 7wt%. Different EDDS dosages from 2Mm to 4Mm influenced the removal efficiency of Cr(VI). This is because EDDS has a high ability to maintain iron in soluble form and played an important role in stabilizing Fe(III) to prevent its precipitation (Dong et al., 2016c). In coupled with the colloidal stability of CS-Fe/Cu, it can be speculated that more surface reactive sites ascribed to a positive effect of the chitosan on the Cr(VI) reduction. In another word, chitosan as a good adsorbent could facilitate accelerate Cr(VI) transfer and adsorb more Cr(VI). However, interestingly, when the chitosan dosages increased from 2 wt% to 4 wt%,

the Cr(VI) reduction efficiency decreased from 95.6% to 90.2% with the increasing dosages of chitosan from 2 wt% to 4 wt%, which suggested that the excessively adsorbed chitosan on the surface of Fe/Cu occupied the active surface sites for Cr(VI) reduction (Zhu et al., 2016). A similar results was recently reported in the study of Starch-nZVI and PAA-nZVI for the adsorption and reduction of Cr(VI) (Shi et al., 2011). Thus, surface stabilizer coating not only affect the colloidal stability but also the reductive activity of nZVI, thus, in the real application, there is a trade off between them should be taken into account. This is essential in guaranteeing that the injected CS-Fe/Cu could transport to the pollutant source zone successfully and removal the heavy metals contaminants efficiently.

On the other hand, the removal efficiency by Fe/Cu was significantly higher than that of nZVI attributed to the galvanic effect of copper (Crane and Sapsford, 2017). This structure favored the generation and transport of electrons which reacted with hexavalent chromium pollutants. The contribution of galvanic effect of copper (4.9%) was slightly lower than that of the dispersant chitosan (9.5%). Most notably, the maximum removal efficiency of 95.6% depended on the synergy effect of copper and chitosan. The contribution of synergy effect (15%) was higher than that of separate function and simple mathematical superposition (14.4%). Thus bimetallic CS-Fe/Cu nanoparticles with dual functional combination galvanic effect of copper and adsorption of chitosan could effectively remove high concertation of hexavalent chromium in wastewater.

3.3 Morphology analysis

3.3.1 SEM characterization

In order to get more direct information about morphology of prepared iron-based materials, SEM micrographs of Fe/Cu and CS-Fe/Cu were obtained, as shown in Fig. 3(a). In the absence of stabilizer chitosan, the SEM image of the freshly prepared Fe/Cu nanoparticles is not very clear because of its strong magnetism. Meanwhile, Fe/Cu nanoparticles were mostly irregular in shape, due to the magnetic forces and high surface tension, the growth and crystallization of Fe/Cu are under the control

(Stefaniuk et al., 2016). In contrast, the stabilized nanoparticles are well dispersed by chitosan as shown in Fig. 3(b) corresponding to low magnification times and Fig. 3(c) corresponding to high magnification times. It can be observed that the surface of CS-Fe/Cu is loose and porous, and the particle structure is favorable for mass transfer from wastewater to the CS-Fe/Cu. Further, the CS-Fe/Cu nanoparticles present smoothly spherical in shape, and these results agree with our previous observation for reduction reactivity due to increased surface areas. These results clearly demonstrated that chitosan played an important role in dispersing bimetallic nanoparticles. In addition, EDX analysis (Fig S1.) along with SEM is very important to analyze the composition of the surface of the sample. 2.69% C derived form the chitosan as a stabilizer. 79.99% Fe is mainly in the form of zero iron as the main component of the chitosan bimetal nanocomposites. 6.72% Cu is used as a component to accelerate electron transfer, which is consistent with the calculated values. Meanwhile, a very small amount of sulfur was detected because the incomplete cleaning process.

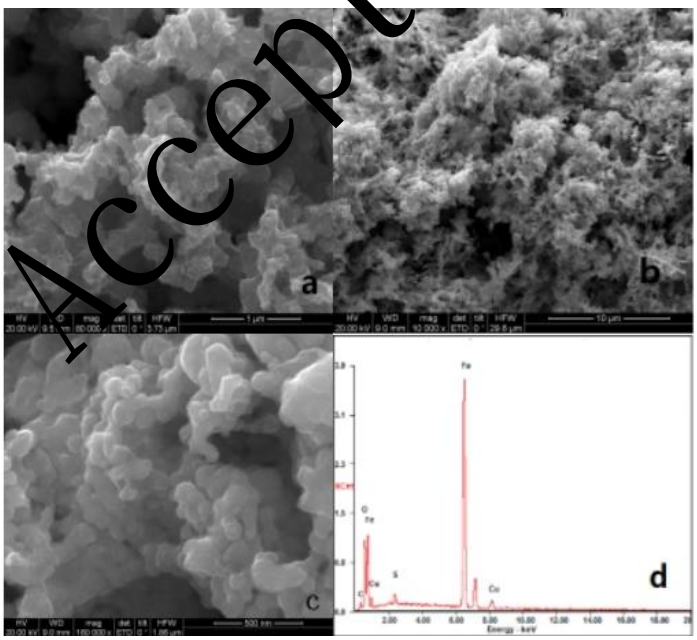

Fig.3. SEM images of (a)Fe/Cu and (b,c) CS-Fe/Cu. EDS spectrum of (d) CS-Fe/Cu.

3.3.2 TEM characterization

The transmission electron micrographs of the Fe/Cu and CS-Fe/Cu nanoparticles as shown in Fig.4. In the absence of chitosan, Fe/Cu nanoparticles formed chain-like

aggregations attributed to the magnetic attractive force, suggesting that it was serious of aggregation, which consistent with XRD. In contrast, CS-Fe/Cu nanoparticles appeared in a fine dispersive state due to the presence of chitosan, as shown in Fig.4 (b). Evidently, the presence of chitosan prevented agglomeration of the resultant nanoparticles, which is confirmed by the above comments on colloidal stability. Apparently, nanoparticle diameter of CS-Fe/Cu was slightly larger than that of Fe/Cu. In addition, the particle diameters were in the range of 50-100 nm, comparable to those reported in the literature. The TEM images of 1.0% Pd-Fe nanoparticles with mean particle diameter are less than 100 nm (Zhu et al., 2016) .

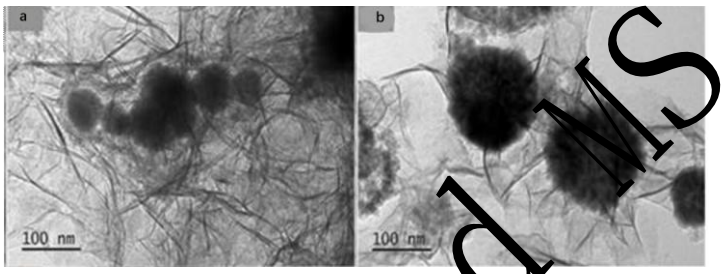

Fig.4. TEM image of SEM images of (a) Fe/Cu ; (b) CS-Fe/Cu.

3.3.3 FTIR characterization

To explain further the stabilization mechanisms of CS-Fe/Cu, FTIR characterization was analyzed for the possible binding sites between chitosan, nZVI and Cu. In the IR Spectrum of chitosan, as shown in Fig.5, a band appeared at 3300-3500 cm^{-1} attributed to O-H stretch. Additional main bands in the presence of chitosan included: bands at 2896, 2780 and 2368 cm^{-1} (C-H strerch); bands at 1022 cm^{-1}(C-O stretch). Meanwhile, a middle strong bands at 1743 and 1380 cm^{-1} represented the typical amide II and amide III of chitosan. Compared to chitosan, the IR characterization spectrum of chitosan, several noticeable vibration changes occurred in the presence of CS-Fe. A broad band at 3413 cm^{-1} distinctly weakened. In addition, the bands at 1743 and 1380 cm^{-1} representing amide II and amide III functional groups significantly weakened. The bands at 1022 cm^{-1} changed correspondingly, which is consistent with the report of Geng (Geng et al., 2009b). The results indicated that nZVI nanoparticles were successfully stabilized by chitosan, and N and O atoms are reactive sites responsible for the connection. Further, the small

amount of Cu had no effect on the CS-Fe, which suggested that there was no obvious interaction between chitosan and copper.

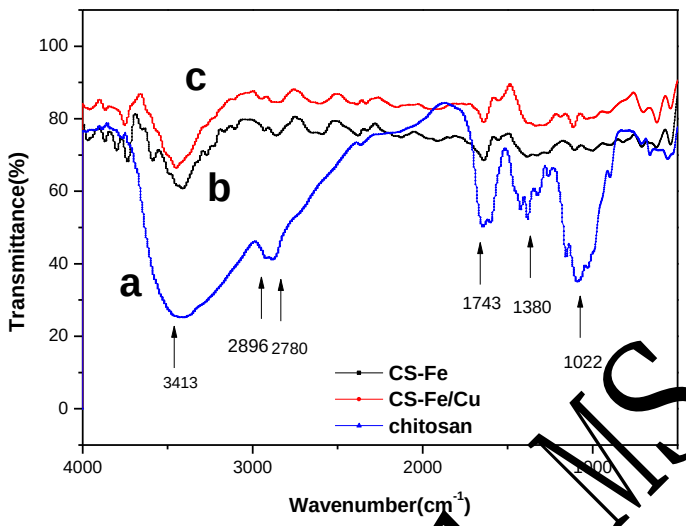

Fig.5. Fourier transform-infrared (FT-IR) spectra of (a) chitosan ; (b) CS-Fe; (c) CS-Fe/Cu.

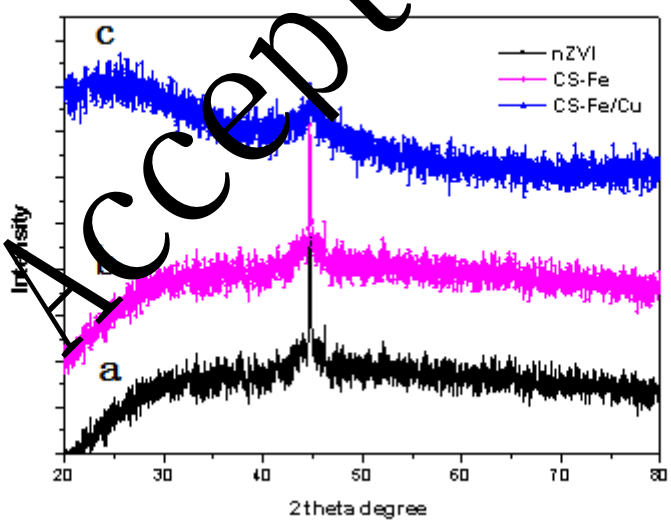

Fig.6. X-ray diffraction analysis of (a) nZVI; (b) CS-Fe; (C) CS-Fe/Cu.

3.3.4 XRD and BET measurement

The XRD patterns of nZVI, CS-Fe and CS-Fe/Cu nanoparticles are presented in Fig.6 (a-c). The strong diffraction peaks of nZVI at 2θ=44.8° can be attributed to

zero-valent iron. In the CS-Fe, the diffraction of nZVI is well preserved. The results demonstrated that chitosan is not only a dispersant responsible for dispering nZVI nanoparticles but also a protectant avoiding the nZVI from oxidation (Geng et al., 2009b). Different from the XRD patterns of nZVI and CS-Fe, the diffraction of nZVI broaden. On the one hand, Fe/Cu bimetallic nanoparticles exist in amorphous form take the place the place of the good crystal shape of nZVI. On the other hand, the copper doping on the surface of Fe reduced the diffraction peak intensity of nZVI. Unfortunately, the diffraction peak of copper is not detected because cooper content is low which not meet the detection limit.

To measure and analyze the specific surface areas of the prepared NPs, N_2 adsorption-desorption isotherms of nZVI and CS-Fe/Cu were provided in supplied materials as shown in Fig S2.. The specific surface areas of the prepared nZVI and CS-Fe/Cu nanocomposites are calculated to be 9.582 and 14.829 m^2/g, respectively. And the increased surface area due to dispersion effect of chitosan contributed to more adsorption sites, which is in agreement with the adsorption performance of the prepared samples in the reduction-adsorption process. And the relative pore volumes of these three samples are 0.050, 0.059 cm^3/g, respectively, which provided a channel for free access of chromium.

3.3.5 TGA

The thermal behavior of the CS-Fe/Cu nanoparticles sample was studied by TGA (Fig.S3). Results showed only one endothermic peak. The weight loss (4.8%) at 400 ℃ was due to decomposition of chitosan, which is consistent of the study of (Horzum et al., 2013).

3.4. Factors affecting on the Cr(VI) reduction

3.4.1 Effects of Cu loading on the Cr(VI) reduction

Except 2wt% chitosan dosage, it is also important to determine the appropriate dosage of copper. In order to investigate the effect of Cu loading on the removal efficiency of Cr(VI), the Cu dosage changed from 1wt% to 5wt% (Cu:Fe, mass fractions), as shown in Fig.S4. The increased Cu dosage from 1wt% to 3wt%

contributed to the increased removal efficiency from 82.3% to 95.6%. When the Cu dosage was up to 5wt%, there was a slight reduction of the removal efficiency of Cr(VI) compared with the highest peak (95.6%). This could be the aggregates of copper nanoparticles due to the excessive dosages. Thus, Cu loading percentage in Fe/Cu nanoparticles of 3.0wt% was chosen as the optical Cu doping dosage.

3.4.2 Effect of initial Cr(VI) concentration on the Cr(VI) reduction

The relation between the initial Cr(VI) concentrations and the apparent rate constant K_{obs} which represents the rate of chemical reaction was studied. As shown in Table 1 and Fig.8., the K_{obs} of the first 20 min is significantly higher than that of the last 40 min, this is due to dominant chemical reduction reaction in the first half of the reaction (Qu et al., 2017), however, physical absorption is responsible for the second half removal of the Cr(VI) regardless of the initial Cr(VI) concentration (Kustov et al., 2011). In the first 20min, the K_{obs} decreased from 14.30×10^{-3} to 12.41×10^{-3} along with the increased the Cr(VI) concentration, and this trend is similar with that the K_{obs} decreased from1.65×10^{-3} to 1.19×10^{-3} in the last 40min along, respectively. In other words, the variation of the rate constant is the opposite of the initial concentration. To the best of our knowledge, Cr(VI) is a strong oxidant and has the passivation effect on the nZVI (Gong et al., 2017b). A complex mixture of $Cr_{0.667}Fe_{0.333}(OH)_3$ and $Cr_{0.667}Fe_{0.333}OOH$ coexistence on the nanoparticle surface will retard the electron transfer from bimetallic nanoparticles to Cr(VI) and accordingly slow down the reaction process (Qian et al., 2017). On the other hand, for a certain amount of adsorbent dosage, referred to limited reactive sites for increased initial Cr(VI) concentration. The results demonstrated that the available active sites of CS-Fe/Cu would be well used even when initial Cr(VI) concentrations are high.

Table 1 Comparison of Cr (VI) K_{obs} for different initial concentrations (CS-Fe/Cu=200 mg/L)

Cr (VI) (mg/L)	K_{obs}(first 20 min)	r^2(first 20 min)	K_{obs}(last 40 min)	r^2(last 40 min)
20.5	14.30×10^{-3}	0.9061	1.65×10^{-3}	0.9087
52.5	13.15×10^{-3}	0.9380	1.30×10^{-3}	0.8279
102.3	12.41×10-3	0.9910	1.19×10-3	0.9756

Table 2 Comparison of Cr (VI) K_{obs} for different temperatures (CS-Fe/Cu=200 mg/L)

Temperature (K)	Kobs(first 20 min)	r2(first 20 min)	Kobs(last 40 min)	r2(last 40 min)
288	12.79×10-3	0.9061	1.08×10-3	0.9102
298	13.00×10-3	0.9380	1.12×10-3	0.8579
303	13.28×10-3	0.9910	1.25×10-3	0.9460

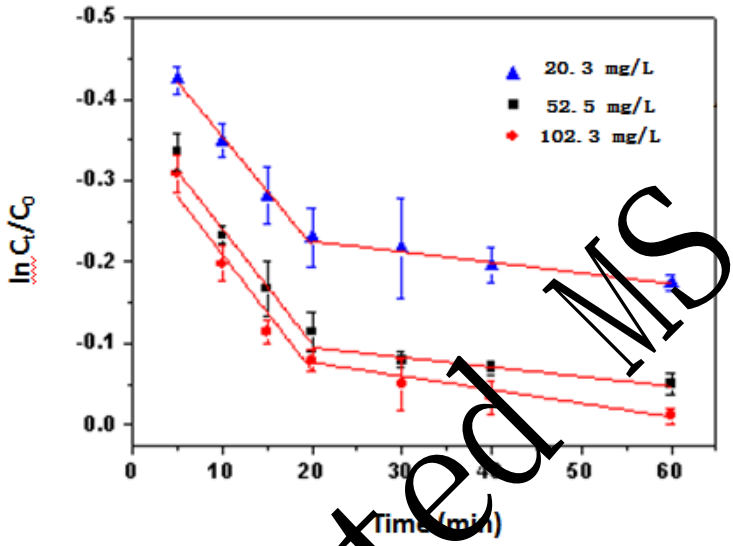

Fig.7. Effect of Cr(VI) concentration on the kinetics of Cr(VI) reduction by CS-Fe/Cu (experiment conditions: CS-Fe/Cu concentration= 200mg/L; Cr(VI) concentration=20.3, 52.5, 102.3 mg/L; pH=7.0).

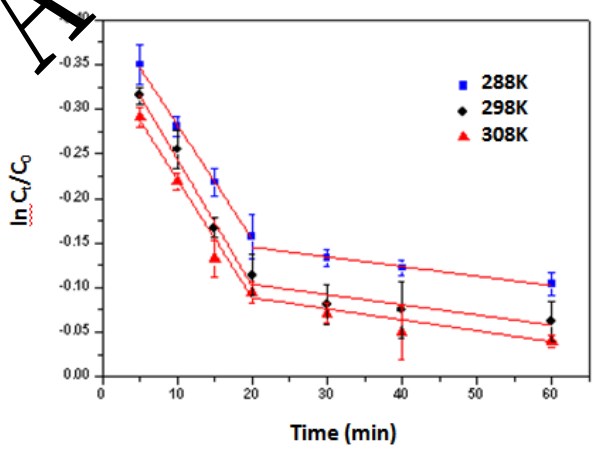

Fig.8 .Effect of temperature on the kinetics of Cr(VI) reduction by CS-Fe/Cu (experiment conditions: Cr(VI) concentration= 20.3mg/L; CS-Fe/Cu concentration:200mg/L;

pH=7.0).

3.4.3 Effect of temperature on the Cr(VI) reduction

The removal of Cr(VI) by CS-Fe/Cu is generally sensitive to temperature. The trend of K_{obs} with a sharp decline and then gentle has been shown in Fig. 8 and table 2. Specially speaking, K_{obs} in the first 20 min was significantly higher than that in the last 40 min, which is similar with that under the different initial Cr(VI) concentration. Meanwhile, there is also a significant trend in K_{obs} as shown in Fig.8, which increased as the temperature increase. Due to the accelerated vibration caused by high temperature, the pollutant quickly shifted from the solution to the surface of the CS-Fe/Cu solid material. In addition, it is an endothermic process and high temperature could provide the energy for the reaction.

3.4.4 Effect of pH on the Cr(VI) reduction

pH is important for the reactivity and life-time of nZVI in water, hence, pH on the apparent rate constant K_{obs} was studied. The reduction of Cr(VI) by CS-Fe/Cu nanoparticles was carried out at pH 3-9, with the initial Cr(VI) concentration of 100 mg/L, CS-Fe/Cu nanoparticles loading of 200 mg/L and at 298K, respectively.

The effects of pH on Cr(VI) removal by Fe/Cu, CS-Fe and CS-Fe/Cu are illustrated in Fig.9 (a), the removal efficiency of Cr(VI) by Fe/Cu were 80.3%, 76.2%, 74.3%, 65.2%, 60.4%, 55%, 50.2% at pH values of 3-9, respectively after 2h. This result indicates the medium pH to a great extent influence the removal efficiency. Such results are intelligible, the reaction between nZVI and Cr(VI) needed and consumed persistently abundant H^+ (Zhou et al., 2015). Hence, under lower pH condition, more available H^+ existed in the aqueous solution that is helpful for Cr(VI) reduction. Meanwhile, the removal efficiency of Cr(VI) in the CS-Fe/Cu system fluctuated in moderation and declined to 86.0% when the pH increased up to 9, which showed that medium pH influenced insignificantly on the Cr(VI) removal efficiency by CS-Fe/Cu. On the other hand, more H^+ help to dissolve passive layer derived from nZVI oxidation and make the reduction reaction constantly progress (Zhou et al., 2016). In addition, the pH variation in the reaction process was also investigated. As shown in Fig.9 (b), it was found that the pH variation in the system increased rapidly within the

initial 20 min, and then tended to stabilize, which is consistent with the above results of K_{obs}. In contrast, the solution pH was alleviated because of the proton of the amine group and less generated hydroxide ions. The above results may relate to the buffering effect of the functional groups on the surface of chitosan, such as hydroxyl groups and amine groups as an excellent proton acceptor (Geng et al., 2009a). Because the reduction of hexavalent chromium requires a large amount of H^+, it lead to increase the pH of the solution. Similarly, Chen et al. reported that sodium dodecyl sulfate (SDS) modified nZVI react with Cr(VI) with the pH of initial solution increased from 2.88 to 8.62 (Huang et al., 2015).

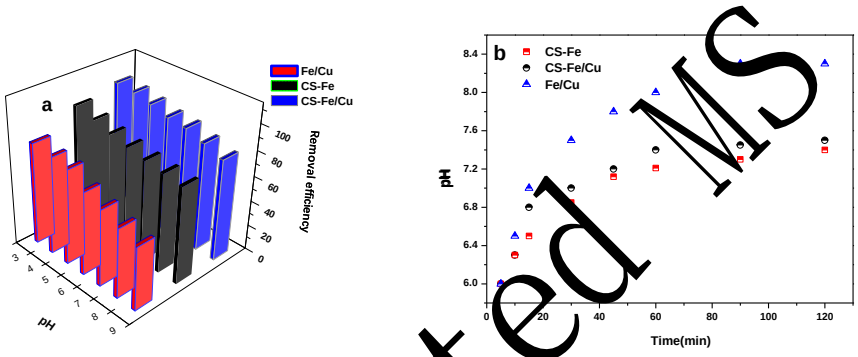

Fig.9. (a) Effect of pH on the removal efficiency of Cr (VI) by Fe/Cu, CS-Fe and CS-Fe/Cu (Cr(VI) concentration=50 mg/L; nanoparticle concentration=200 mg/L) and (b) the variation of pH during Cr(VI) reaction in Fe/Cu, CS-Fe and CS-Fe/Cu systems.

3.5. Comparison of the degradation of Cr(VI) in natural samples

In the real applications, the composition of actual wastewater is extremely complex. Therefore, the differences could be obtained on the Cr(VI) removal efficiency between the simulated waterwater and an actual polluted wasterwater. In this work, the removal efficiency of Cr(VI) by CS-Fe/Cu from ultrapure water, river water (Xiangjiang River, Changsha), tannery wastewater (Leath goods factory, Changsha), smelting waterwater (Smelting plant, Zhuhzou) were studied, as shown in Fig.S5. The results showed that the Cr(VI) removal efficiency is 96%, 90% and 85% for ultrapure water, river water and tannery water, however, relatively lower removal of Cr(VI) (80%) was observed in smelting wastewater, this is because other heavy metals as oxidants competitive with Cr (VI). The results suggested that CS-Fe/Cu has a great potential for the real Cr(VI) wasterwater.

3.6 Mechanistic interpretations

The above-described experimental results demonstrated that CS-Fe/Cu is an efficient dual-functional nanomaterial for Cr(VI) wasterwater. To best of our knowledge, various mechanisms have been explained for removal of heavy metal ions in aqueous solution by nZVI. Because of the difference of standard potential of heavy metal, nZVI immobilized heavy metal mechanisms include reduction, complex formation, electrostatic adsorption, precipitation and co-reaction (Z et al., 2017). To further explain the Cr(VI) removal mechanism, the elemental compositions and valence states of nZVI and the resultant CS-Fe/Cu composites were characterized by XPS. The whole region scan of the nZVI and CS-Fe/Cu surface after reaction with the Cr(VI) contaminated aqueous solution as show in Fig. S6. After the reaction, new characteristic peaks around 580 ev emerged corresponding to chromium appeared, which suggested the uptake of Cr(VI) on the surface of iron-based nanoparticles (Xiong et al., 2016). In addition, compare to nZVI, more obvious absorption spectrum of Cr(VI) can be seen, which is consistent with the more active activity of nZVI.

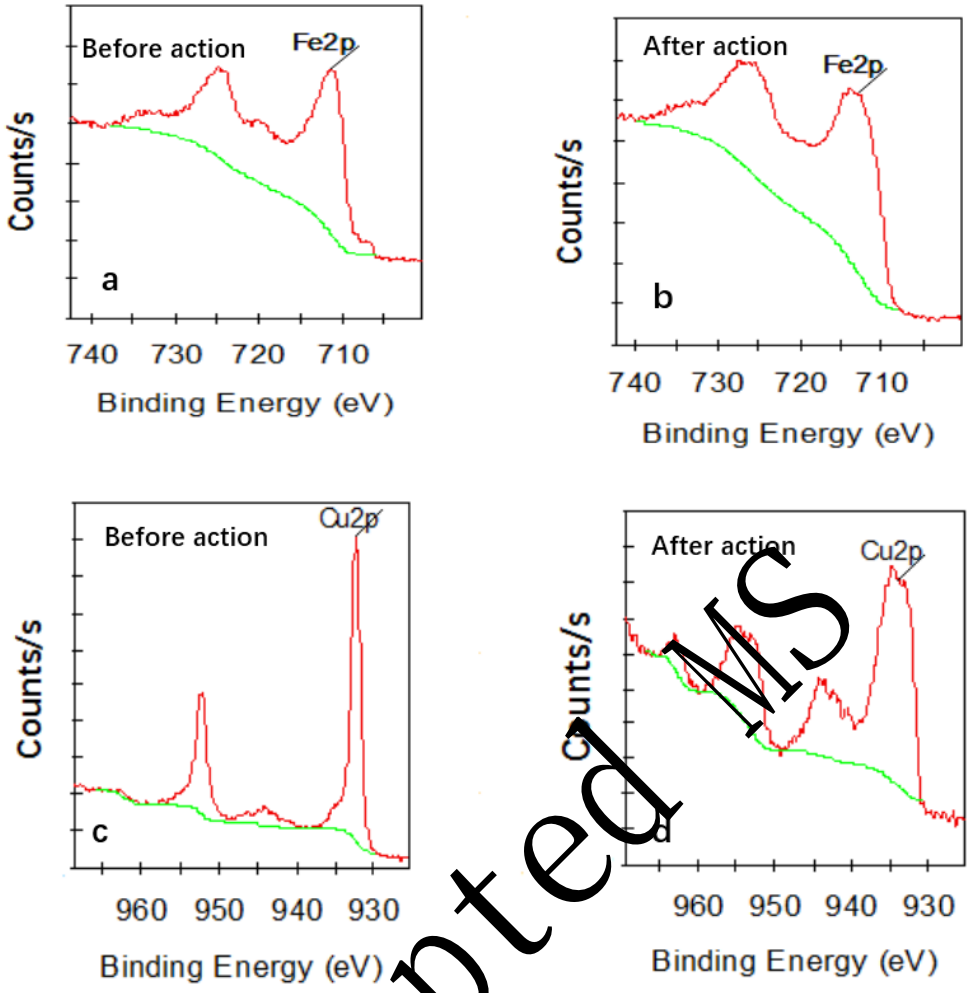

Fig. 10. XPS spectra of Fe2p and Cu2p from CS-Fe/Cu before and after reaction with Cr(VI), a Fe 2p before action; b Fe 2p after reaction; c Cu 2p before action; d Cu 2p after action.

To illustrate the role of chitosan and Cu in the Cr(VI) removal, firstly, the XPS Cr 2p spectrum of Fe/Cu and CS-Fe/Cu was compared, as shown in Fig. S7. The spin-orbit splitting of 9.8 eV are chracteristic of Cr(III) (Hu et al., 2011). For the Fe/Cu, the existence of chromium was in the form of Cr(III) and Cr(VI). The results showed that the incomplete reduction of Fe/Cu. On the one hand, the oxidation products covered the surface of Fe/Cu prevented the electron from transferring to the Cr(VI) (Soliemanzadej and Fekri., 2017). On the other hand, the chitosan played an important role in the adsorption of Cr (VI) due to the chelation. Therefore, the uptake of chormium in the form of trivalent and hexavalent exist on the surface of Fe/Cu. Compare to Fe/Cu, the Cr(III) as the only existence form existed on the surface of CS-Fe/Cu, which suggested that the complete reduction of

Cr(VI). On the one hand, the electrons constantly transferred from the nZVI to Cr(VI) because of the synergistic effect of chitosan and copper. On the other hand, completely oxidation of nZVI may attribute to the free N-H and O-H groups of chitosan, which bind with Fe(III) and inhibit the Fe(III)-Cr(III) co-precipitate formation (Naim et al., 2016).

Secondly, the detailed XPS spectrum of Fe and Cu before and after the reaction was significant for the explanation of the reaction mechanism. As can be seen form the Fig. 10. (a,b), before the reaction, Fe existed in the form of zero valence and trivalent, which suggested that the zero-valent iron has some degree of oxidation. After the reaction, iron is oxidized into trivalent iron attributed to the contributed electrons. Compare to Fe, Cu may existed in the form of Cu2O or Cu as can seen in Fig. 10. (c), before the reaction, which is different from the study of Nakseedee (Nakseedee et al. 2016). Form the XANES psecra of Cu K-edge, it revealed that $(Cu\text{-}Fe)_{IS}$ (corresponded to the situ synthesis method) possessed only Cu_2O phase while $(Cu\text{-}Fe)_{IM}$ (corresponded to the impregnation synthesis method) contained a mixed phase of Cu_2O and CuO. However, after the reaction, Cu existed in the form of CuO which is consistent with that was verified by the LCF analysis AS, as shown in Fig. 10. (d). Thus, Cu_2O before the reaction converted to CuO after the reaction. The phenomen include precipitation and coprecipitation phenomena. The removal process is started with Cu^{2+} acting as an electron transfer to accept electron from Fe^0, resulting in Fe^{2+} and iron (hydr) oxides (FexOy) formation. The reaction proceeds continuously to cover all part of copper particles. At this point, Cr is removed readily by a coprecipiation with FexOy (Hu et al. 2010). Thus, the adsorption effect of chitosan as well as the precipitation and coprecipitation of copper are responsible for the Cr(VI) reduction, as shown in Fig. 11.

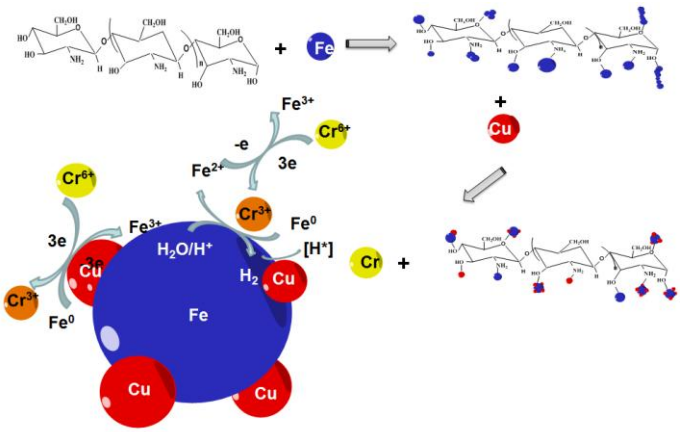

Fig.11 The hypothesis of the possible synthesis process of chitosan-stabilized Fe/Cu and removal mechanism of Cr(VI)

4. Conclusion

In this study, bimetallic Fe/Cu nanopartilces were prepared and successfully stabilized by chitosan for the removal of hexavalent chromium from wastewater. There is a compromise between the stabilization and the reactivity of nZVI because of the effect of surface coating, and the best dosage of chitosan and Cu in this study is 2wt% and 3wt%, respectively. This is confirmed by SEM and TEM images, nanomaterials existed in an uniform dispersed form. XRD and FTIR analysis revealed that CS-Fe/Cu has good stability against oxidation. In addition, CS-Fe/Cu have the maximum Cr(VI) removal efficiency higher than all of nZVI, Fe/Cu and CS-Fe/Cu, attributed to the syntactical effects of increased specific surface areas and the galvanic cell. CS-Fe/Cu have a high removal efficiency of Cr(VI) under the high initial Cr(VI) concentration in a wide range of pHs of 3-9. The XPS analysis explained the role of chitosan and Cu in the Cr(VI) removal, the results demonstrated that the possible removal mechanisms could be simultaneous adsorption of chitosan and precipitation and coprecipitation of Cu. In summary, this study demonstrates a great potential of CS-Fe/Cu for heavy metal removal.

Acknowledgments

This study was financially supported by the National Natural Science Foundation of China (51521006, 51378190, 51278176, 51408206, 51579098 and 51579096), the National Program for Support of Top-Notch Young Professionals of China (2012,

2014), the Program for New Century Excellent Talents in University (NCET-13-0186), Scientific Research Fund of Hunan Provincial Education Department (521293050), the Program for Changjiang Scholars and Innovative Research Team in University (IRT-13R17).

Reference

Arancibia-Miranda N, Baltazar SE, García A, Muñoz-Lira D, Sepúlveda P, Rubio MA, et al. Nanoscale zero valent supported by Zeolite and Montmorillonite: Template effect of the removal of lead ion from an aqueous solution. Journal of Hazardous Materials 2016; 301: 371-380.

Crane RA, Sapsford DJ. Selective formation of copper nanoparticles from acid mine drainage using nanoscale zerovalent iron particles. Journal of Hazardous Materials 2017.

Dong H, Guan X, Wang D, Ma J. Individual and combined influence of calcium and anions on simultaneous removal of chromate and arsenate by Fe(II) under suboxic conditions. Separation and Purification Technology 2011; 80: 284-292.

Dong H, Jiang Z, Deng J, Zhang C, Cheng Y, Hou K, et al. Physicochemical transformation of Fe/Ni bimetallic nanoparticles during aging in simulated groundwater and the consequent effect on contaminant removal. Water Research 2017a: 51-57.

Dong H, Qi H, Zeng G, Lin T, Chang Z, Xie Y, et al. Chromate removal by surface-modified nanoscale zero-valent iron: Effect of different surface coatings and water chemistry. Journal of Colloid & Interface Science 2016a; 471: 7-13.

Dong H, Xie Y, Zeng G, Lin T, Jie L, Qi H, et al. The dual effects of carboxymethyl cellulose on the colloidal stability and toxicity of nanoscale zero-valent iron. Chemosphere 2016b; 144: 1682-1689.

Dong H, Zeng Y, Xie Y, He Q, Zhao F, Wang Y, et al. Single and combined removal of Cr(VI) and Cd(II) by nanoscale zero-valent iron in the absence and presence of EDDS. Water Science and Technology 2017b; 76: 1261-1270.

Dong H, Zeng Y, Zeng G, Huang D, Liang J, Zhao F, et al. EDDS-assisted reduction of Cr(VI) by nanoscale zero-valent iron. Separation & Purification Technology 2016c; 165: 86-91.

Dong H, Zhao F, He Q, Xie Y, Zeng Y, Zhang L, et al. Physicochemical transformation of carboxymethyl cellulose-coated zero-valent iron nanoparticles (nZVI) in simulated groundwater under anaerobic conditions. Separation & Purification Technology 2017c; 175: 376-383.

Feng J, Lim TT. Pathways and kinetics of carbon tetrachloride and chloroform reductions by nano-scale Fe and Fe/Ni particles: comparison with commercial micro-scale Fe and Zn. Chemosphere 2005; 59: 1267.

Gao Y, Wang F, Wu Y, Naidu R, Chen Z. Comparison of degradation mechanisms of microcystin-LR using nanoscale zero-valent iron (nZVI) and bimetallic Fe/Ni and Fe/Pd nanoparticles. Chemical Engineering Journal 2016; 285: 459-466.

Geng B, Jin Z, Li T, Qi X. Kinetics of hexavalent chromium removal from water by chitosan-Fe0 nanoparticles. Chemosphere 2009a; 75: 825-830.

Geng B, Jin Z, Li T, Qi X. Preparation of chitosan-stabilized Fe0 nanoparticles for removal of hexavalent chromium in water. Science of The Total Environment 2009b; 407: 4994-5000.

Gong X, Huang D, Liu Y, Zeng G, Wang R, Wan J, et al. Stabilized Nanoscale Zerovalent Iron

Mediated Cadmium Accumulation and Oxidative Damage of Boehmeria nivea (L.) Gaudich Cultivated in Cadmium Contaminated Sediments. Environ Sci Technol 2017a; 51: 11308-11316.

Gong Y, Gai L, Tang J, Fu J, Wang Q, Zeng EY. Reduction of Cr(VI) in simulated groundwater by FeS-coated iron magnetic nanoparticles. Science of The Total Environment 2017b; 595: 743-751.

Horzum N, Demir MM, Nairat M, Shahwan T. Chitosan fiber-supported zero-valent iron nanoparticles as a novel sorbent for sequestration of inorganic arsenic. RSC Advances 2013; 3: 7828.

Hu CY, Lo SL, Liou YH, Hsu YW, Shih K, Lin CJ. Hexavalent chromium removal from near natural water by copper-iron bimetallic particles. Water Res 2010; 44: 3101-8.

Hu XJ, Wang JS, Liu YG, Li X, Zeng GM, Bao ZL, et al. Adsorption of chromium (VI) by ethylenediamine-modified cross-linked magnetic chitosan resin: isotherms, kinetics and thermodynamics. Journal of Hazardous Materials 2011; 185: 306-314.

Huang D, Xue W, Zeng G, Wan J, Chen G, Huang C, et al. Immobilization of Cd in river sediments by sodium alginate modified nanoscale zero-valent iron: Impact on enzyme activities and microbial community diversity. Water Research 2016; 106: 15-25.

Huang DL, Chen GM, Zeng GM, Xu P, Yan M, Lai C, et al. Synthesis and Application of Modified Zero-Valent Iron Nanoparticles for Removal of Hexavalent Chromium from Wastewater. Water Air & Soil Pollution 2015; 226: 375.

Kazemi MO, Jahanshahi M, Peyravi M. Hexavalent chromium removal by multilayer membrane assisted by photocatalytic couple nanoparticle from both permeate and retentate. Journal of Hazardous Materials 2017.

Kumar MA, Bae S, Han S, Chang Y, Lee W. Reductive dechlorination of trichloroethylene by polyvinylpyrrolidone stabilized nanoscale zerovalent iron particles with Ni. Journal of Hazardous Materials 2017; 340: 399.

Kumarathilaka P, Jayaweera V, Wijesekara H, Kottegoda IRM, Rosa SRD, Vithanage M. Insights into Starch Coated Nanozero Valent Iron-Graphene Composite for CrVI Removal from Aqueous Medium. Journal of Nanomaterials,2016,(2016-11-16) 2016; 2016: 7.

Kustov LM, Finashina ED, Shuvalova EV, Tkachenko OP, Kirichenko OA. Pd-Fe nanoparticles stabilized by chitosan derivatives for perchloroethene dechlorination. Environment International 2011; 37: 1044.

Li H, Ge Y, Zhang X. High efficient removal of lead from aqueous solution by preparation of novel PPG-nZVI beads as sorbents. Colloids & Surfaces A Physicochemical & Engineering Aspects 2016; 513.

Li J, Zhang X, Sun Y, Liang L, Pan BC, Zhang W, et al. Advances in Sulfidation of Zerovalent Iron for Water Decontamination. Environmental Science & Technology 2017a; 248: 173-182.

Li Y, Li X, Han D, Huang W, Yang C. New insights into the role of Ni loading on the surface structure and the reactivity of nZVI toward tetrabromo- and tetrachlorobisphenol A. Chemical Engineering Journal 2017b; 311: 173-182.

Liang DW, Yang YH, Xu WW, Peng SK, Lu SF, Xiang Y. Nonionic surfactant greatly enhances the reductive debromination of polybrominated diphenyl ethers by nanoscale zero-valent iron: mechanism and kinetics. Journal of Hazardous Materials 2014; 278: 592-596.

Ling L, Huang XY, Li M, Zhang WX. Mapping the Reactions in a Single Zero-valent Iron Nanoparticle. Environmental Science & Technology 2017; 51: 14293-14300.

Liu F, Shan C, Zhang X, Zhang Y, Zhang W, Pan B. Enhanced removal of EDTA-chelated Cu(II) by polymeric anion-exchanger supported nanoscale zero-valent iron. Journal of Hazardous Materials 2017; 321: 290-298.

Liu T, Yang X, Wang ZL, Yan X. Enhanced chitosan beads-supported Fe(0)-nanoparticles for removal of heavy metals from electroplating wastewater in permeable reactive barriers. Water Research 2013; 47: 6691.

Lv Y, Niu Z, Chen Y, Hu Y. Bacterial effects and interfacial inactivation mechanism of nZVI/Pd on Pseudomonas putida strain. Water Research 2017; 115: 297-308.

Naim MM, El-Shafei AA, Elewa MM, Moneer AA. Application of silver-, iron-, and chitosan-nanoparticles in wastewater treatment. International Conference of European Desalination Society, Desalination for Environment: Clean Water and Energy, 2016, pp. 268–280.

Nakseedee P, Tanboonchuy V, Khemthong P, Grisdanurak N, Liao CH. Role of Cu on zero valent bimetallic Cu—Fe in arsenic removal with gas bubbling. Environmental Progress & Sustainable Energy 2017.

Peng Z, Xiong C, Wei W, Tan F, Yang X, Wang X, et al. Facile modification of nanoscale zero-valent iron with high stability for Cr(VI) remediation. Science of the Total Environment 2017; s 596–597: 266-273.

Qian L, Zhang W, Yan J, Han L, Chen Y, Ouyang D, et al. Nanoscale zero-valent iron supported by biochars produced at different temperatures: Synthesis mechanism and effect on Cr(VI) removal. Environmental Pollution 2017; 223: 153-160.

Qu G, Kou L, Wang T, Liang D, Hu S. Evaluation of activated carbon fiber supported nanoscale zero-valent iron for chromium (VI) removal from groundwater in a permeable reactive column. Journal of Environmental Management 2017; 201: 378-387.

Shi L-n, Zhang X, Chen Z-l. Removal of Chromium (VI) from wastewater using bentonite-supported nanoscale zero-valent iron. Water Research 2011; 45: 886-892.

Soliemanzadeh A, Fekri M. The application of green tea extract to prepare bentonite-supported nanoscale zero-valent iron and its performance on removal of Cr(VI): Effect of relative parameters and soil experiments. Microporous & Mesoporous Materials 2017; 239: 60-69.

Stefaniuk M, Oleszczuk P, Yong SO. Review on nano zerovalent iron (nZVI): From synthesis to environmental applications. Chemical Engineering Journal 2016; 287: 618-632.

Tian H, Liang Y, Zhu T, Zeng X, Sun Y. Surfactant-enhanced PEG-4000-NZVI for remediating trichloroethylene-contaminated soil. Chemosphere 2018; 195: 585-593.

Xie Y, Dong H, Zeng G, Zhang L, Cheng Y, Hou K, et al. The comparison of Se(IV) and Se(VI) sequestration by nanoscale zero-valent iron in aqueous solutions: The roles of solution chemistry. Journal of Hazardous Materials 2017; 338: 306-312.

Xie Y, Yi Y, Qin Y, Wang L, Liu G, Wu Y, et al. Perchlorate degradation in aqueous solution using chitosan-stabilized zero-valent iron nanoparticles. Separation & Purification Technology 2016; 171: 164-173.

Xiong K, Gao Y, Zhou L, Zhang X. Zero-valent iron particles embedded on the mesoporous silica–carbon for chromium (VI) removal from aqueous solution. Journal of Nanoparticle Research 2016; 18: 267.

Xu P, Zeng GM, Huang DL, Feng CL, Hu S, Zhao MH, et al. Use of iron oxide nanomaterials in wastewater treatment: a review. Sci Total Environ 2012; 424: 1-10.

Xue W, Huang D, Zeng G, Wan J, Zhang C, Xu R, et al. Nanoscale zero-valent iron coated with

rhamnolipid as an effective stabilizer for immobilization of Cd and Pb in river sediments. Journal of Hazardous Materials 2017; 341: 381.

Zeng G, Chen M, Zeng Z. Risks of neonicotinoid pesticides. Science 2013; 340: 1403.

Zeng Y, Walker H, Zhu Q. Reduction of nitrate by NaY zeolite supported Fe, Cu/Fe and Mn/Fe nanoparticles. Journal of Hazardous Materials 2017; 324: 605.

Z L, L W, J M, X L, J X, F W, et al. Zeolite-supported nanoscale zero-valent iron: New findings on simultaneous adsorption of Cd(II), Pb(II), and As(III) in aqueous solution and soil. Journal of Hazardous Materials 2017; 344: 1-11.

Zhou J, Sun Q, Chen D, Wang H, Yang K. Ochrobactrum anthropi used to control ammonium for nitrate removal by starch-stabilized nanoscale zero valent iron. Water Science & Technology A Journal of the International Association on Water Pollution Research 2017; 76: 1827.

Zhou X, Lv B, Zhou Z, Li W, Jing G. Evaluation of highly active nanoscale zero-valent iron coupled with ultrasound for chromium(VI) removal. Chemical Engineering Journal 2015; 281: 155-163.

Zhou Y, Tang L, Yang G, Zeng G, Deng Y, Huang B, et al. Phosphorus-doped ordered mesoporous carbons embedded with Pd/Fe bimetal nanoparticles for the dechlorination of 2,4-dichlorophenol. Catalysis Science & Technology 2016; 6: 1930-1939.

Zhu BW, Lim TT, Feng J. Reductive dechlorination of 1,2,4-trichlorobenzene with palladized nanoscale Fe 0 particles supported on chitosan and silica. Chemosphere 2006; 65: 1137-1145.

Zhu F, Li L, Ma S, Shang Z. Effect factors, kinetics and thermodynamics of remediation in the chromium contaminated soils by nanoscale zero valent Fe/Cu bimetallic particles. Chemical Engineering Journal 2016; 302: 663-669.